JOURNAL OF GEOPHYSICAL RESEARCH, VOL. 115, B06307, doi:10.1029/2009JB006332, 2010

S wave velocity structure below central Mexico using high-resolution surface wave tomography

A. Iglesias,[1] R. W. Clayton,[2] X. Pérez-Campos,[1] S. K. Singh,[1] J. F. Pacheco,[1,3] D. García,[1] and C. Valdés-González[1]

Received 26 January 2009; revised 15 December 2009; accepted 11 January 2010; published 15 June 2010.

[1] Shear wave velocity of the crust below central Mexico is estimated using surface wave dispersion measurements from regional earthquakes recorded on a dense, 500 km long linear seismic network. Vertical components of regional records from 90 well-located earthquakes were used to compute Rayleigh-wave group-velocity dispersion curves. A tomographic inversion, with high resolution in a zone close to the array, obtained for periods between 5 and 50 s reveals significant differences relative to a reference model, especially at larger periods (>30 s). A 2-D *S* wave velocity model is obtained from the inversion of local dispersion curves that were reconstructed from the tomographic solutions. The results show large differences, especially in the lower crust, among back-arc, volcanic arc, and fore-arc regions; they also show a well-resolved low-velocity zone just below the active part of the Trans Mexican Volcanic Belt (TMVB) suggesting the presence of a mantle wedge. Low densities in the back arc, inferred from the low shear wave velocities, can provide isostatic support for the TMVB.

Citation: Iglesias, A., R. W. Clayton, X. Pérez-Campos, S. K. Singh, J. F. Pacheco, D. García, and C. Valdés-González (2010), *S* wave velocity structure below central Mexico using high-resolution surface wave tomography, *J. Geophys. Res.*, *115*, B06307, doi:10.1029/2009JB006332.

1. Introduction

[2] The geometry of the subducted Cocos plate below central Mexico and the crustal structure of the region have been topics of research ever since it was recognized that a segment along the coastal area of the region is a seismic gap [*Kelleher et al.*,1973; *Singh et al.*, 1981]. This segment, which is called the Guerrero seismic gap, poses significant seismic hazard to some coastal towns, including Acapulco, and to Mexico City. A detailed knowledge of the plate geometry and the velocity structure is important in understanding the dynamics of the subduction zone. This knowledge is also critical in understanding amplification of seismic waves as they propagate toward Mexico City and in the estimation of ground motions in the region during future earthquakes [e.g., *Ordaz and Singh*, 1992]. Early studies, based on seismicity and focal mechanisms, revealed that Cocos plate initially subducts below Mexico at a shallow angle and then becomes subhorizontal and remains so up to a distance of about 200 km from the coast, where it reaches a depth of about 50 km [e.g., *Suárez et al.*, 1992; *Singh and Pardo*, 1993; *Pardo and Suárez*, 1995].

[3] Crustal velocity structure in central Mexico has been studied by *Valdés-González and Meyer* [1996], *Campillo et al.* [1996], and *Iglesias et al.* [2001], among others. *Valdés-González and Meyer* [1996] reported that the oceanic plate subducts with a constant angle of 10° from the trench. *Campillo et al.* [1996] inverted a logarithmic stack of group-velocity dispersion curves of nine earthquakes located near the Guerrero coast that were recorded in Mexico City and obtained an average *S* wave velocity model of the crustal structure perpendicular to the coast. *Iglesias et al.* [2001] stacked dispersion curves for paths perpendicular and parallel to the coast and found significant difference between the two paths in the period range of 5 to 35 s.

[4] To better image the subducted Cocos plate, an array of 100 broadband seismographs, with a spacing of ~5 km, was deployed along a line perpendicular to the Middle America Trench (MAT) during 2004–2006. This array, which is called the Middle America Subduction Experiment (MASE) array, extended from the Pacific coast of Mexico near Acapulco to almost the Gulf of Mexico (Figure 1). An extensive analysis of receiver functions and teleseismic *P* wave tomography, using MASE data, confirms flat subduction of the Cocos plate in the distance range of ~150 to 300 km inland from MAT, beyond which it plunges into the mantle with a dip of ~75° [*Pérez-Campos et al.*, 2008]. The slab is imaged to a depth of ~500 km. The Moho is well defined along the line and shows that the crust is thicker in the back arc than in the fore arc. Although receiver functions are sensitive to impedance contrasts, they cannot be used to obtain the absolute velocity structure because of

[1]Departamento de Sismología, Instituto de Geofísica, Universidad Nacional Autónoma de México, Mexico City, Mexico.
[2]Seismological Laboratory, California Institute of Technology, Pasadena, California, USA.
[3]Observatorio Vulcanológico y Sismológico de Costa Rica, Heredia, Costa Rica.

0148-0227/10/2009JB006332

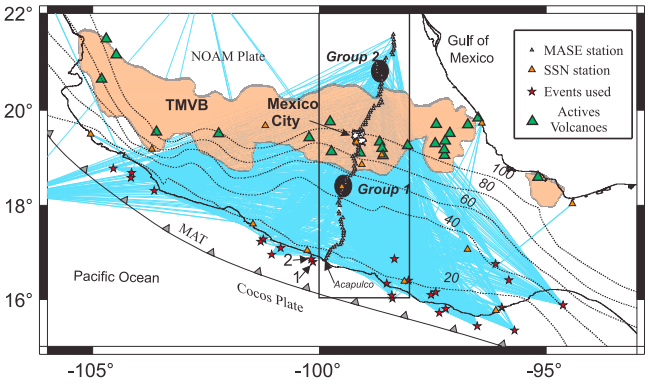

Figure 1. Map showing the study area. The orange area shows the Trans Mexican Volcanic Belt (TMVB). Black dashed lines indicate isodepths of Cocos plate [after *Pardo and Suárez*, 1995]. Vertical rectangle delineates the region where our study has resolution (see text). Blue lines are the paths at the period T of 20.48 s. Stars and numbers 1 and 2 are regional earthquakes referred in the text. Groups 1 and 2 are subsets of fore-arc and back-arc receivers, respectively.

the trade-off between depth and velocity [e.g., *Yanovskaya*, 1984; *Julià et al.*, 2000]. In this paper, we complement the receiver function study with surface wave dispersion measurements from regional events to determine the *S* wave velocity structure along the MASE profile. We supplement the MASE data with stations of the National Seismological Service (SSN) of Mexico.

2. Data and Processing

[5] The steps followed in this work consisted of group-velocity measurements from regional data in section 2.1, tomographic inversion of a set of path-average group-velocity measurements and resolution tests in section 2.2, forward test for consistency in section 2.3, and reconstruction of local dispersion curves and inversion for crustal structure in section 2.4.

2.1. Group-Velocity Measurements From Regional Data

[6] Since the method used in this study is sensitive to the accuracy of epicentral location, we only used earthquakes that occurred within 50 km of a seismic station. For relocation purposes, we also used records from the strong motion network operated by Instituto de Ingeniería, Universidad Nacional Autónoma de México (UNAM). This network is especially dense over the Guerrero seismic gap [*Anderson et al.*, 1994]. SSN reported 303 earthquakes in Mexico with $M \geq 4.5$ during December 2004 to April 2007. Of these events, we could relocate 90 with an RMS < 0.5 s. Group velocities of the fundamental-mode Rayleigh wave were measured on the vertical-component seismograms at MASE and SSN stations. We used the frequency-time analysis proposed by *Levshin et al.* [1989] to obtain dispersion curves (5–50 s) for each event-station combination. More than 6000 dispersion curves were computed. Low signal/noise ratio and instrumental problems prevented us from obtaining clear dispersion curves over the entire 5–50 s range. The average dispersion curves of *Iglesias et al.* [2001] for coastal and perpendicular paths were taken as reference curves. Each computed dispersion curve was individually analyzed and compared with the two reference curves. The periods at which the curves were clearly inconsistent with the reference curves were discarded. This procedure resulted on an average of 975 paths at each period. Table 1 lists the number of paths at each selected period. Figure 1 shows the geographical distribution of the paths at $T = 20.48$ s.

2.2. Tomographic Inversion of a Set of Path-Average Group-Velocity Measurements and Resolution Tests

[7] The procedure described in section 2.1 resulted in a set of path-average group-velocity measurements between an epicenter and a station. We applied a tomographic scheme [e.g., *Julià et al.*, 2000] to find a 2-D group-velocity map for each period. An optimized continuous regionalization algorithm [*Debayle and Sambridge*, 2004] was used to

Table 1. Number of Valid Paths for Each Period

Period (s)	Number of Valid Paths
5.00	493
5.24	497
5.51	511
5.80	564
6.07	629
6.36	664
6.69	708
6.97	759
7.28	798
7.71	838
8.09	872
8.40	887
8.86	903
9.23	909
9.78	919
10.24	1001
10.74	937
11.30	954
11.70	1026
12.37	957
12.85	960
14.25	994
14.89	1024
15.60	1001
16.38	1072
17.25	1010
18.20	1014
18.72	1006
19.86	1007
20.48	1142
21.85	1013
22.60	1005
24.27	998
25.21	1011
26.21	994
27.31	1117
28.50	984
31.21	956
32.77	979
34.50	944
36.41	950
38.55	922
40.96	1040
43.69	883
46.81	880
50.41	827
Average	*975*

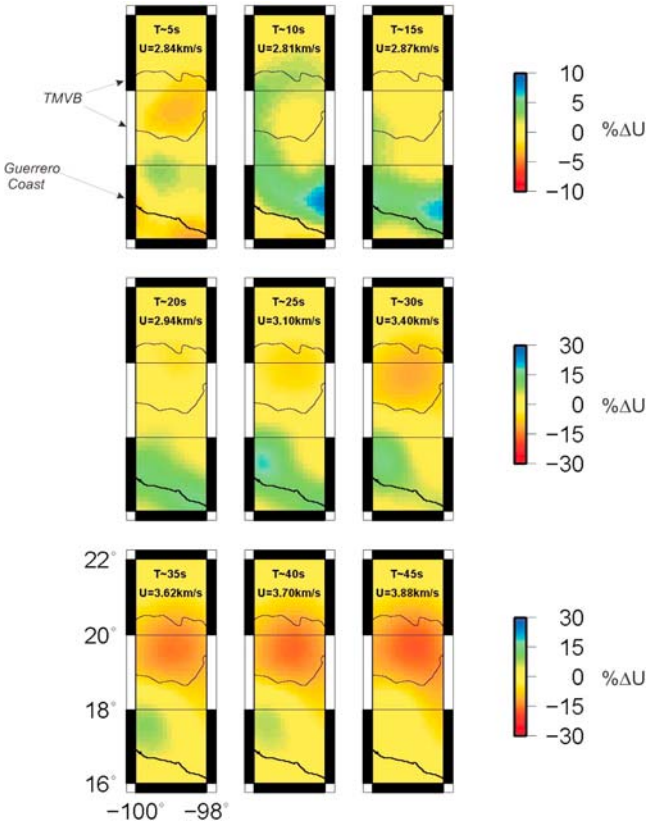

Figure 2. Tomographic averaged images of relative group velocities (ΔU) at selected periods presented as a percentage of perturbation of the reference Raleigh-wave group-velocity model.

invert the set of group velocities at each period. The algorithm uses a continuous formulation of the inverse problem and a least squares criterion. A Gaussian a priori covariance function controls the degree of horizontal smoothing in the inverted model.

[8] In our problem, the region was initially discretized as a regular mesh of 1/8° × 1/8°. We chose the average Rayleigh-wave dispersion curve obtained by *Iglesias et al.* [2001] for paths perpendicular to the coast as initial model and performed a separate tomographic inversion at each period.

[9] A bootstrap procedure [*Efron and Tibshirani*, 1993] was used to test data stability. We made 20 individual replications for each period choosing, randomly, N paths, where N is the available number of paths for the period. Then we averaged the 20 replications for each square of the grid.

[10] Figure 2 shows the averaged tomographic images of group velocities at periods between ~5 s and ~45 s, with a step of 5 s. The images are presented as a perturbation of the reference group velocity.

[11] Following the methodology proposed by *Debayle and Sambridge* [2004], the resolution tests of the tomographic inversions are evaluated using Voronoi diagrams. In our problem, the region is initially discretized as a regular mesh of 1/8° × 1/8° (~14 km × ~14 km); this represents the "initial Voronoi Diagram." A criterion based on the path distribution in each cell is used to determine whether a node of the diagram has a possibility to be randomly erased or not (see details in [*Debayle and Sambridge*, 2004]). After erasing some nodes of the initial configuration, a new Voronoi Diagram is built. The process is iterative and stops when the criterion is satisfied in all cells. Figure 3 shows the results of this analysis for a period of ~20 s. It also shows the standard deviation obtained from the bootstrap procedure.

[12] The reliability of tomographic images increases near the MASE line, as expected, and the resolution at the tips, especially at the northern part of the line, decreases considerably. Hence we chose a narrow band close to the MASE line, 16–20.5°N and 98–100°W, for detailed analysis.

2.3. A Forward Test for Consistency

[13] In order to validate the tomographic images described above, we used two coastal earthquakes whose locations were roughly aligned with the MASE array (events 1 and 2 in Figure 1). Following the procedure of *Shapiro et al.* [1997], we computed stacked Rayleigh-wave dispersion curves of these two events recorded on two groups of stations. Stations in Group 1 are located in the fore arc, while those in Group 2 are located in the back arc (Figure 1). Figure 4 shows some examples of individual dispersion curves for each path and the result of the stacking procedure.

[14] As Figure 5 shows, the stacked dispersion curves for the two groups are very different from each other and from the curve for the reference model (solid line in Figure 5 (top) and 5 (bottom)), indicating a significant lateral variation in the shear wave velocities. Forward modeling of the tomographic problem, using the group-velocity images in Figure 2, was applied to compute average dispersion curves to Group 1 stations in the fore arc (solid triangles in Figure 5, top) and to Group 2 stations in the back arc (solid triangles in Figure 5, bottom). The reasonable agreement between the curves and the corresponding dots indicates that the tomographic model adequately represents the lateral variations.

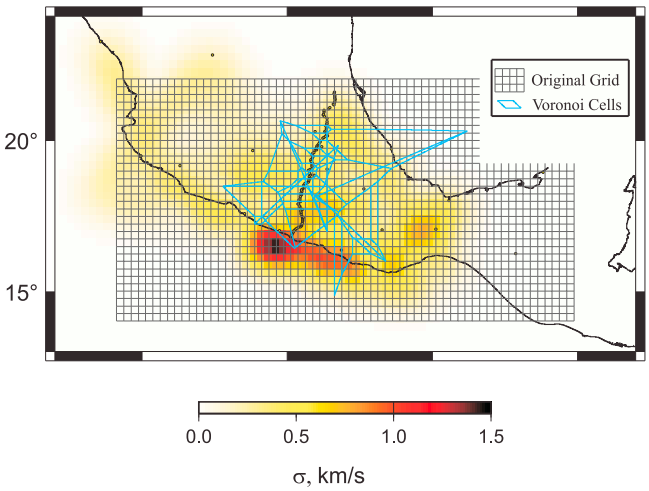

Figure 3. Resolution test for T = 20.48 s. The light gray grid represents the initial configuration for the resolution test. The blue solid lines give a final configuration after the test. Colors represent standard deviation computed from the 20 individual replications in the bootstrap process (see text).

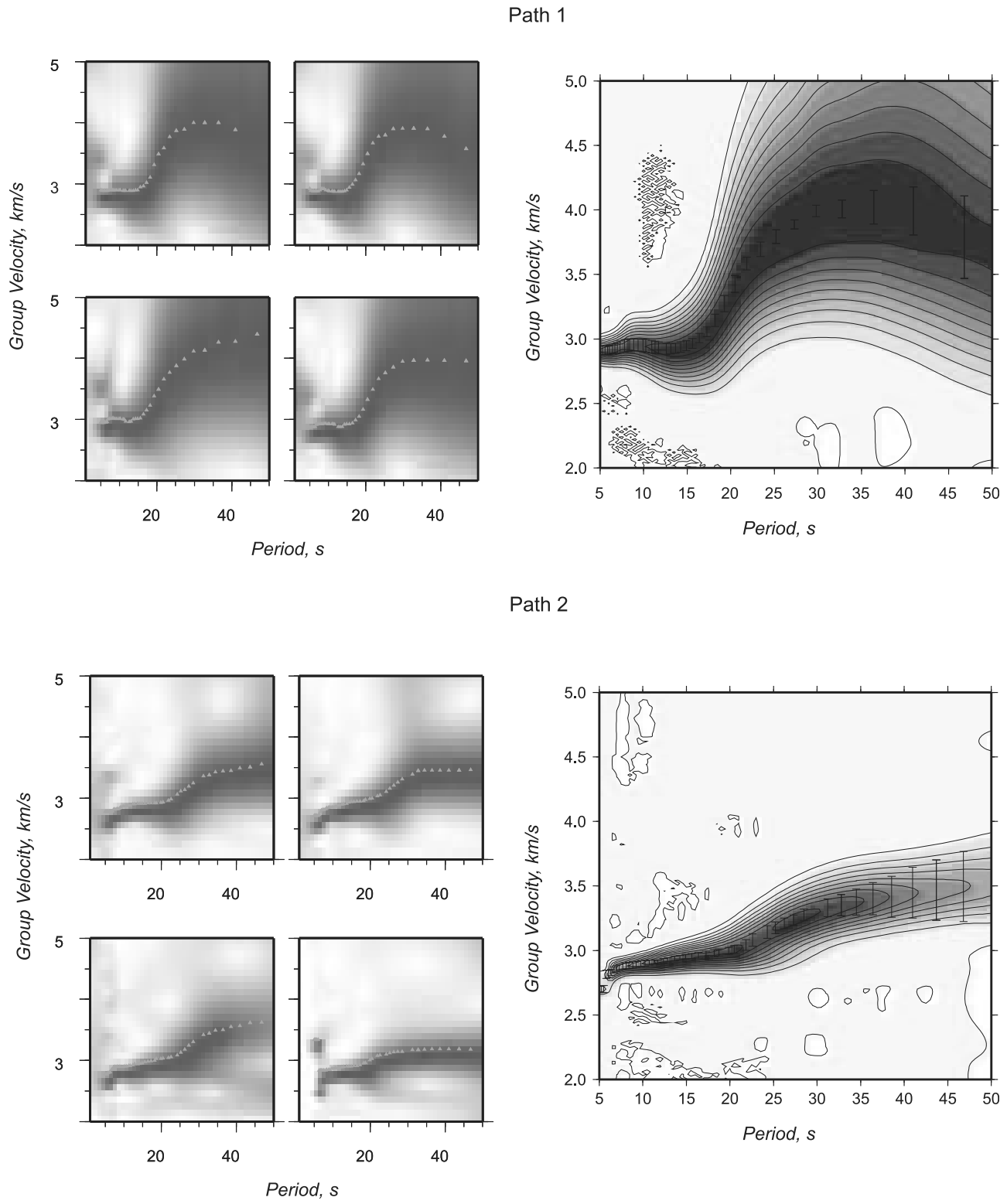

Figure 4. (top) Path 1. (left) Dispersion curves obtained for some stations of Group 1. (right) Stacked dispersion curve for Group 1. (bottom) Same as Figure 4 (top) but for path 2.

2.4. Local Dispersion Curves and Inversion for Crustal Velocity Models

[15] From the computed average tomographic images (Figure 2), we reconstructed "local" dispersion curves for each MASE station. We transferred uncertainties on tomographic images derived from the bootstrap procedure to local dispersion curves as uncertainties for each period. We, then, individually inverted local dispersion curves at several periods between 5 and 45 s to find velocities and thicknesses

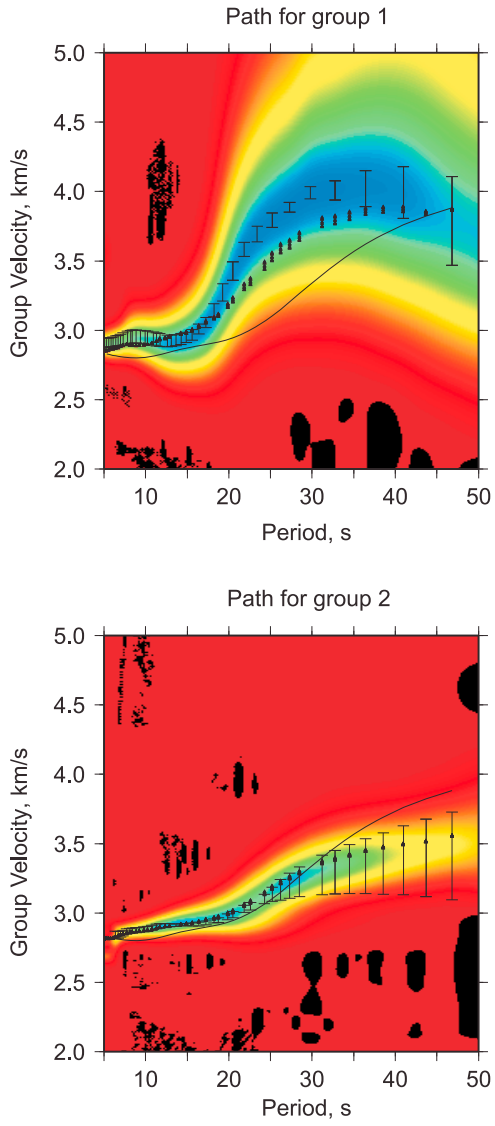

Figure 5. Comparison of dispersion curves computed by forward modeling of local group-velocity tomographic images (triangles; see text) and stacked observed dispersion curves for events 1 and 2 (Figure 1) at stations from (top) Group 1 (coast-fore arc) and (bottom) Group 2 (coast-back arc). Solid line is the theoretical dispersion curve for the model used as reference [*Iglesias et al.*, 2001].

of a three-layer over a half-space model. Misfit was computed using the following L2 norm [*Menke*, 1984]:

$$E = \sqrt{\sum_{n} \left(\overline{U_i^0} - U_i^P(\beta_{1..4}, h_{1..4}) \right)^2},$$

where $\overline{U_i^0}$ is the average group velocity for the i period, $U_i^p(\beta_{1\ldots4}, h_{1\ldots3})$ is the predicted group velocity depending on the combination of β, h in the three-layer over half-space model, and n is the total number of periods.

[16] Following the procedure of *Iglesias et al.* [2001], we used a simulated annealing algorithm to minimize E. In the inversion, we fixed Poisson's ratio as $v = 0.25$ and computed density from the following relation: $\rho = 0.32\alpha + 0.77$, where ρ is in g/cm^3 and α is in km/s [*Berteussen*, 1977]. Inversion of surface wave dispersion curves is a nonlinear and nonunique problem, and the solution could depend on the initial model and parameterization [e.g., *Pedersen et al.*, 2009].

[17] To reduce the nonuniqueness of the problem, we fixed the depth of the Moho to that reported by *Pérez-Campos et al.* [2008] for the back-arc zone of the model, whereas for the fore arc we fixed the depth of the third layer, where the basement of the continental crust is well resolved in the same work (diamonds in Figure 6).

[18] To compute uncertainties for the resulting parameters (βs, and hs), we retained not only the "best fitted model" during the inversion but also a set of models that lie within the area bounded by $\overline{U_i^p} \pm (2\sigma)$. However, between stations 55 and 80, this procedure would not yield any model lying inside the error band at longer periods (>30 s, see Figure 7). To have a qualitative solution for these stations, we kept some models even though they were outside the error band.

[19] Figure 6 shows the interpolation along the MASE line of average *S* wave velocity models (red lines in Figure 7) inverted for each station.

[20] Local dispersion curves and the fits for the selected models at some MASE stations are shown in Figure 7.

3. Discussion

[21] As Figure 5 demonstrates, there is a significant difference between dispersion curves for the fore-arc and the back-arc stations. This difference is clearly observed in tomographic images of group velocities, especially at periods ≥20 s (Figure 2). Although the active volcanoes are located in the southern part of the Trans Mexican Volcanic Belt (TMVB), low group-velocity regions at T = 20 and 25 s, which are shown by red spots, appear at the northern end of the TMVB. The red spots at these periods coincide with a shallow anomalously high-conductivity region reported by *Jodicke et al.* [2006] from a magnetotelluric study that was carried out along a profile almost coincident with the MASE array. The fact that the high-conductivity, low-velocity region does not coincide with the area of the active volcanoes is puzzling. *Jodicke et al.* [2006] suggest three possible mechanisms to explain the anomaly: fossil partial melt and associated metamorphic fluids, fluid in a major shear zone, and graphitic shear zones in the middle and lower crust.

[22] At $30 \leq T \leq 45$ s, the low-velocity red spots cover the whole TMVB. We attribute this to the presence of a low-velocity mantle wedge (Figure 6). The largest group-velocity contrast (±25%) occurs around T = 30 s. Around this period, a large blue-green spot covers the region between the coast and the southern limit of the TMVB (Figure 2), which is most probably related to the presence of relatively high-velocity subducted oceanic mantle below the fore arc (Figure 6).

[23] For most of the profile, the assumed model is enough to explain dispersion curves. Inversion finds a shallow interface (<10 km depth and ~3.3 km/s) and a thin crust for about 150 km from the coast (Figure 6). As mentioned above, in the inversion, we fixed the Moho depth to that reported by *Pérez-Campos et al.* [2008]: a thin continental

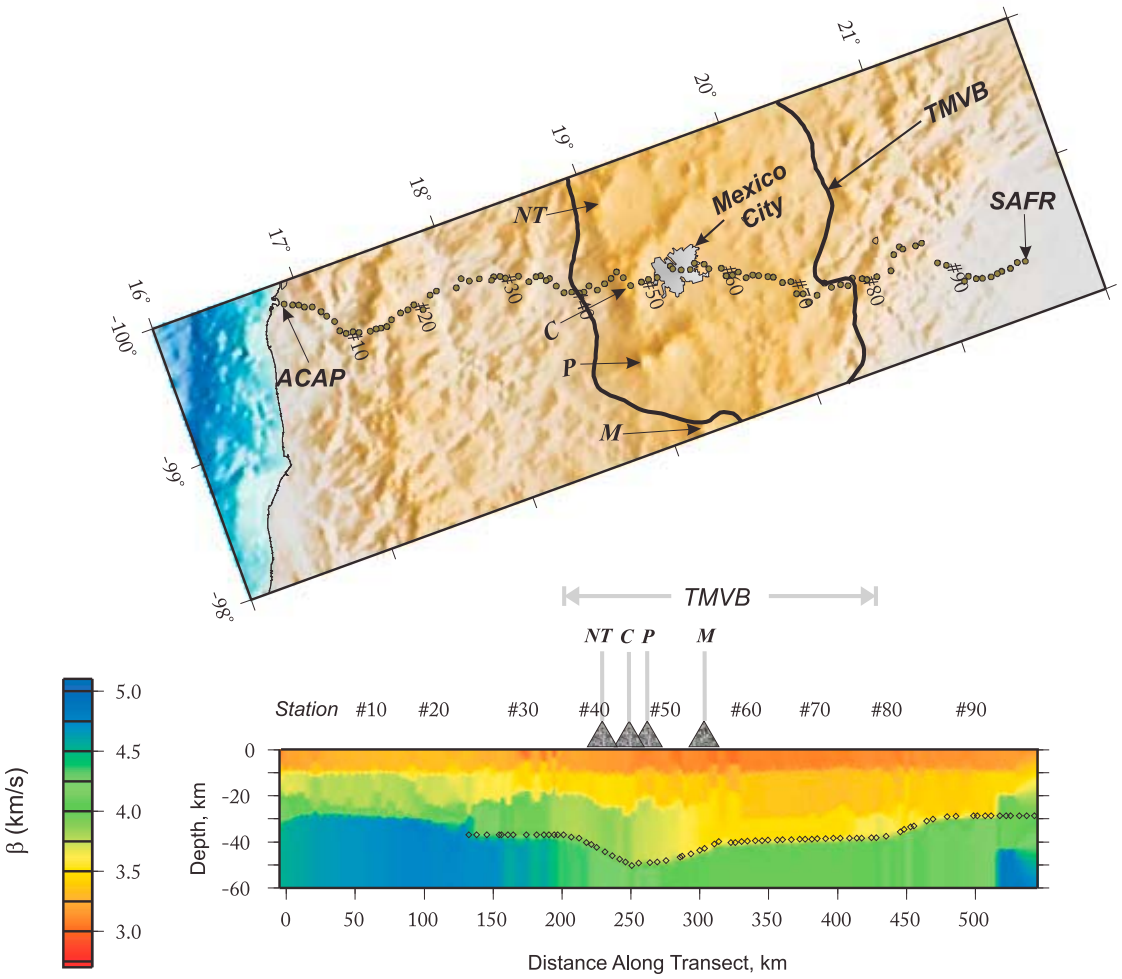

Figure 6. (top) Location of MASE stations (dots) and main volcanoes. NT, Nevado de Toluca; C, Chichinautzin field; P, Popocatépetl; M, Malinche. (bottom) *S* wave velocity section for the MASE transect obtained from the inversion of local dispersion curves. Stations are numbered from ACAP (Acapulco Station) (station 1) in the South to SAFR (San Francisco Station) (station 100) in the North. Diamonds show Moho's location [after *Pérez-Campos et al.*, 2008]. The crust in the fore arc is thinner and faster than in the back-arc region. A low-velocity zone below the TMVB (light green) could be related to the presence of a mantle wedge.

crust (~30 km) for about 150 km from the coast that gets thicker, reaching ~45 km, just below the highest topographic point. In the northern part of the profile, the crust is thicker than in the fore-arc region (<30 km). *Pérez-Campos et al.* [2008] used the International Association of Seismology and Physics of the Earth's Interior (IASPEI) 91 model to back project the receiver functions to convert the time axis to depth. Comparing the IASPEI 91 model with the model obtained from the inversion of local dispersion curves (Figure 7), we note that they are very similar around station 30 (~175 km from coast); the *S* wave velocities, however, are consistently higher for stations close to the coast and lower for stations in the TMVB. *Pérez-Campos et al.* [2008] report a low-velocity, 10 km thick layer just below the continental crust in the fore-arc region. We performed forward tests to probe the sensitivity of the dispersion curves to this low-velocity layer and found slight variations in the period interval of 10–25 s (Figure 8). These variations could not be resolved with our methodology.

[24] The shear wave velocities of the lower crust and the mantle are distinctly faster in the fore arc as compared to the back arc (Figure 6). The low velocity below the southern part of the TMVB is probably associated with a hot mantle wedge.

[25] One of the proposed mechanisms to uplift the Colorado Plateau is hydration of the lithosphere by the flat subduction during the Laramide Orogeny [*Humphreys et al.*, 2003]. In this mechanism, the additional water would come from the slab and would cause partial melting in the lithosphere, which would have the effect of reducing the shear wave speed and the density there. *Li et al.* [2002] show that low densities inferred from low shear wave speeds in the crust beneath the Rocky Mountains can provide isostatic support for this feature. The situation in central Mexico along the MASE is similar except, of course, the orogeny is still in progress. If a similar mechanism is occurring here, one would expect a reduced shear velocity in the TMVB where the rollback of the slab has occurred.

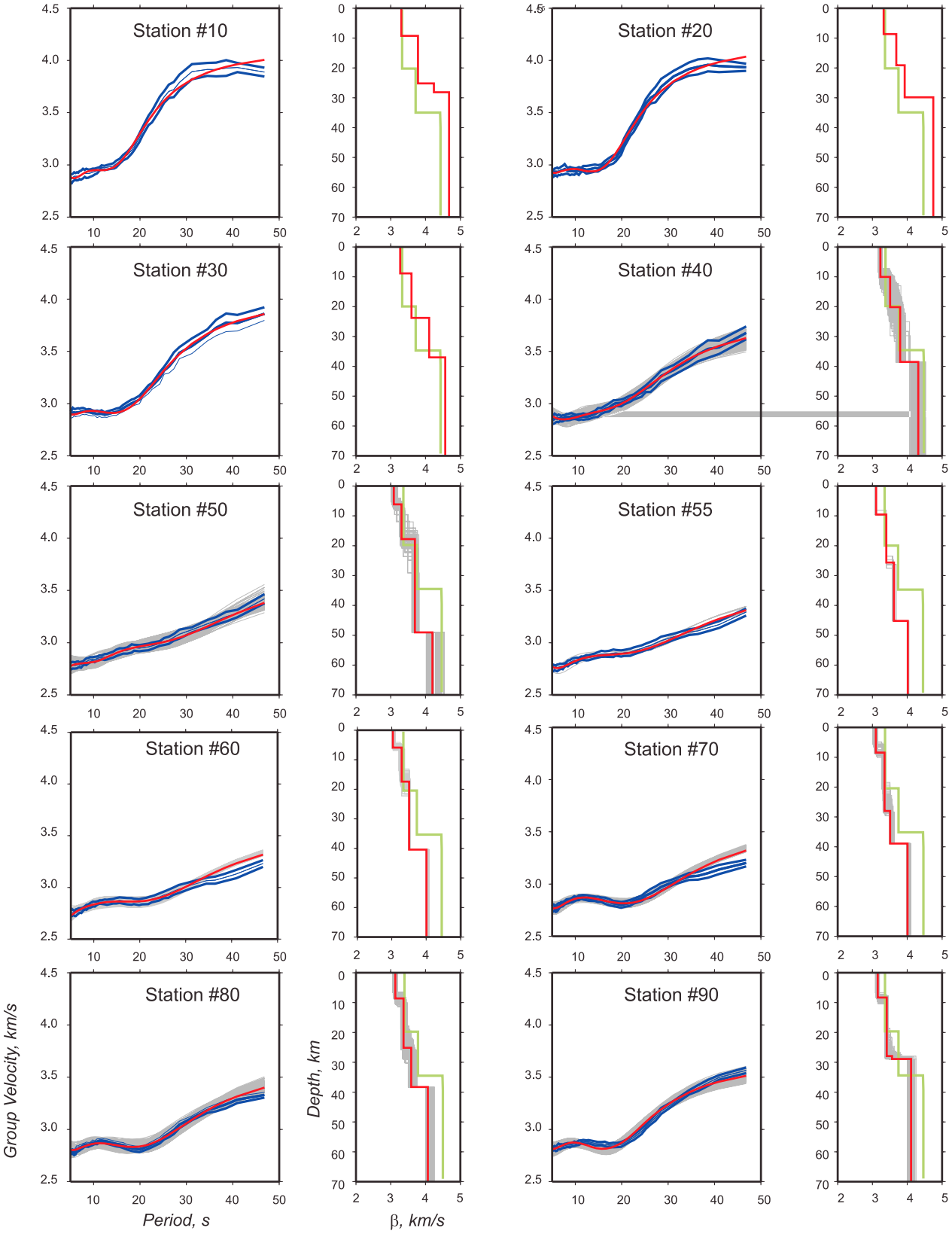

Figure 7. (left) Examples of fit, for selected models (gray lines), to some local dispersion curves. Red line is the theoretical dispersion curve for the average model and blue lines represent $\overline{U_i^p} \pm \sigma$. (right) The selected models along the inversion (gray lines), average model computed from selected models (red line), and IASPEI 91 *S* wave velocity models (green line). Stations are numbered from Acapulco (station 1) in the South to SAFR (station 100) in the North.

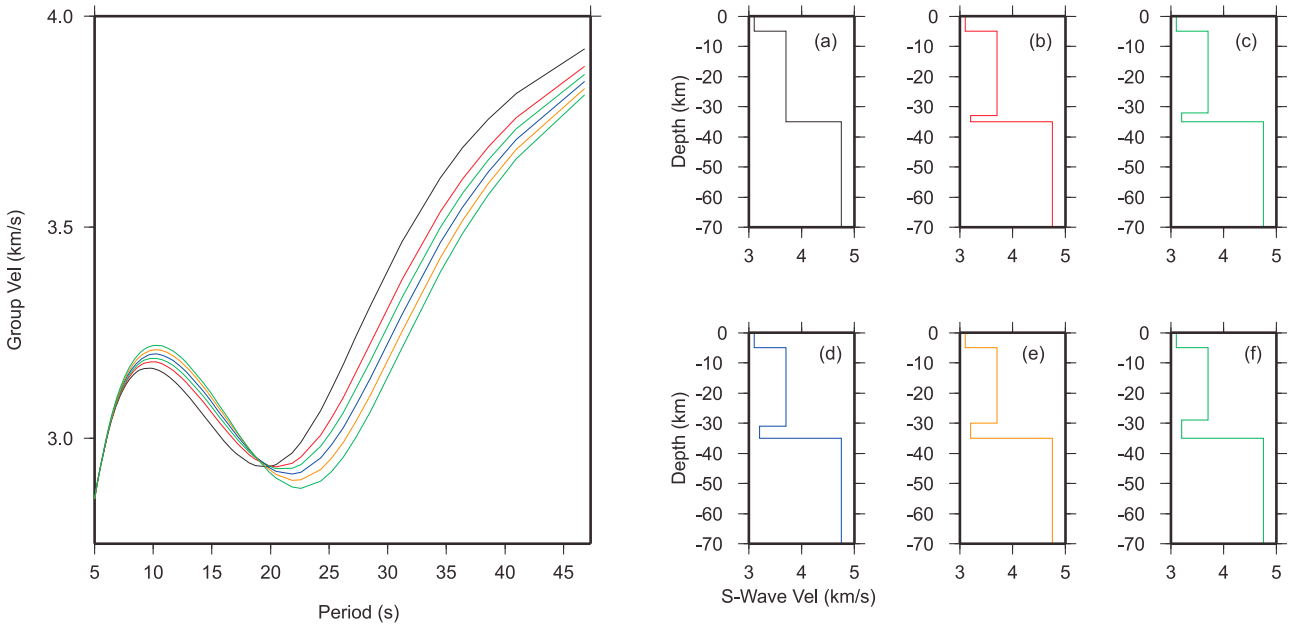

Figure 8. Sensitivity Rayleigh-wave dispersion curves to the presence of a low-velocity layer at the base of the crust of varying thickness. (a) h = 0 km. (b) h = 2 km. (c) h = 3 km. (d) h = 4 km. (e) h = 5 km. (f) h = 6 km. The dispersion curves are shown on the left.

[26] This reduction in shear velocity can be used as a proxy for density reduction and consequently be used to predict the uplift that would occur. The elevation changes can be predicted assuming Pratt compensation mechanism and a linear relationship between density and shear velocity changes. To determine the variations in shear velocity, a reference profile was constructed from measured shear velocity in the fore arc at 150 km from the coast (station 30 in Figure 6) where the topography is approximately flat. Anomalous elevation relative to this point is calculated with a standard Pratt model with a compensation depth of 45 km (the approximate Moho depth for most of the model). The analysis was also done with a variable depth of compensation (i.e., the measured depth of Moho), but this made little difference to the results. The predicted uplift curves do a reasonable job of matching the TMVB uplift. The topography at 80 km from the coast (the 30 Ma arc) is not fit by this model presumably because its elevation is not related to the current flat slab geometry and hence the crust was not hydrated as suggested for the TMVB. The two ends of the model are also not well fit because of poor resolution of the shear velocity model.

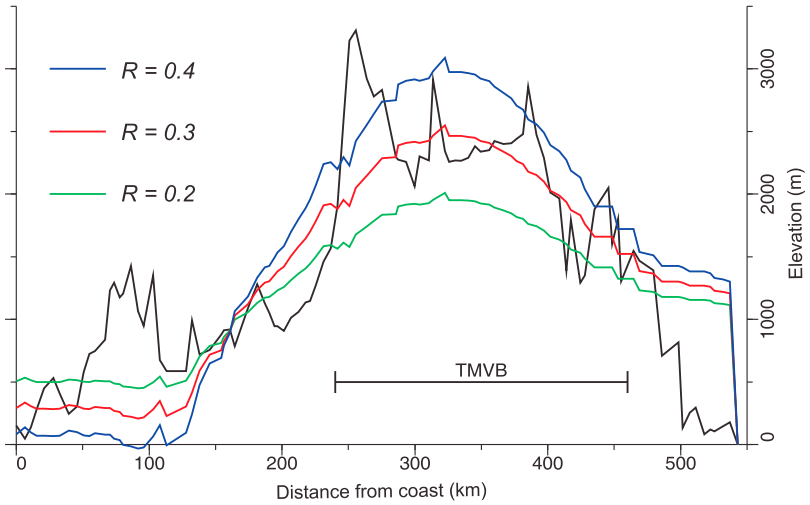

Figure 9. Elevation of the TMVB predicted from shear velocity variations. The black curve is the topography along the MASE line. The three curves are for different ratios (R) of density variation to shear velocity variation of 0.2 (green), 0.3 (red), and 0.4 (blue), where $R = \partial \ln\rho / \partial \ln\beta$. The Cenozoic arc at 80 km is not fit because its elevation is due to a different mechanism.

[27] In Figure 9, we show the predicted values of uplift for values of the ratio between density variations and shear-speed variations of 0.2, 0.3, and 0.4. The best fit is for 0.3. The value of these parameters is not well constrained [*Deschamps et al.*, 2001] but is within the experimental and theoretical ranges.

[28] The velocity structure in Figure 6 is consistent with the estimated Q in the region. Higher crustal velocity in the fore-arc region as compared to the TMVB agrees with higher Q of Lg waves in the former ($Q = 273f^{0.66}$ [*Ordaz and Singh*, 1992]) as compared to the latter region ($Q = 98f^{0.72}$ [*Singh et al.*, 2007]). The low-velocity mantle below the TMVB is associated with relatively low Q ($Q = 80f^{0.82}$ [*Singh et al.*, 2006]). An analysis of attenuation of body waves along the MASE line by *Chen and Clayton* [2009] shows a low-Q zone extending from the TMVB until the northern part of the line. Low Q in this region correlates with low S wave velocity for the crust found in the present work.

4. Conclusions

[29] The geometry of the MASE array was designed to image the subducted Cocos plate below central Mexico. For this reason, the stations were installed in a line perpendicular to the trench (Figure 1). Although this geometry is not ideal for surface wave tomography, in the present study, we complemented the MASE array with permanent stations of the National Seismological Service (SSN) and obtained reliable and detailed images of Rayleigh-wave group velocity at periods between 5 and 50 s in a narrow rectangular area centered at the MASE transect. The main characteristic of tomographic images is a low-velocity spot at $T \geq 20$ s, which covers the TMVB (Figure 2). This low-velocity region most probably corresponds to the mantle wedge, since it is located in the region where the plate starts bending and sinking into the continental mantle at a steep angle [*Pérez-Campos et al.*, 2008]. The group-velocity contrast between fore arc and back arc is clearly seen in Figure 5, where for $T > 15$ s the average Rayleigh-wave dispersion curve for the path from Guerrero coast to TMVB and that corresponding to the path from the coast to the end of the TMVB are significantly different.

[30] From tomographic images, we reconstructed "local" dispersion curves for each MASE station and obtained a 2-D S wave velocity model using simulated annealing inversion. This velocity model shows contrast of +15% and −30% with respect to that reported by *Iglesias et al.* [2001], which was obtained from inversion of stacked average Rayleigh-wave group-velocity dispersion curve for a path between Guerrero coast and Mexico City. The model shows that the crust in the fore arc is thinner and faster than in the back arc. A very low velocity zone, below the southern part of the TMVB (depth >40 km), is required to fit our local dispersion curves. This zone is most probably related to the presence of a hot mantle wedge.

[31] **Acknowledgments.** This study was supported by the Tectonics Observatory of Caltech and by the PAPIIT-UNAM project IN104308. MASE was funded by the Gordon and Betty Moore Foundation. We thank E. Debayle and M. Sambridge for providing their tomographic and resolution codes. O. A. Castro kindly assisted us in relocating some of the events used in this study. We thank S. I. Franco-Sánchez for the help in preparing the last versions of Figures 6 and 7. SSN and C.I.S., I.I., UNAM staff generously provided us seismic data from their networks. We thank all MASE volunteers, most of them undergraduate students. Finally, we thank the JGR Editor and two anonymous reviewers for their comments and suggestions that led to a much improved manuscript. Contribution 91 of the Tectonics Observatory.

References

Anderson, J. G., J. N. Brune, J. Prince, R. Quaas, S. K. Singh, D. Almora, P. Bodin, M. Oñate, R. Vásquez, and J. M. Velasco (1994), The Guerrero accelerograph network, *Geofis. Int.*, *33*, 341–372.

Berteussen, K. A. (1977), Moho depth determination based on spectral ratio analysis of NORSAR long-period *P* waves, *Phys. Earth Planet. Inter.*, *31*, 313–326.

Campillo, M., S. K. Singh, N. Shapiro, J. Pacheco, and R. B. Hermann (1996), Crustal structure of the Mexican volcanic belt, based on group velocity dispersion, *Geofis. Int.*, *35*(4), 361–370.

Chen, T. and R.W. Clayton (2009), Seismic attenuation structure in central Mexico: Image of a focussed high-attenuation zone in the mantle wedge, *J. Geophys. Res.*, *114*, B07304, doi:10.1029/2008JB005964.

Debayle, E., and M. Sambridge (2004), Inversion of massive surface wave data sets: Model construction and resolution assessment, *J. Geophys. Res.*, *109*, B02316, doi:10.1029/2003JB002652.

Deschamps, F., R. Snieder, and J. Trampert (2001), The relative density-to-shear velocity scaling in the uppermost mantle, *Phys. Earth Planet. Inter.*, *124*, 193–221, doi:10.1016/S0031-9201(01)00199-6.

Efron, B., and R. J. Tibshirani (1993), *An Introduction to the Bootstrap, Monogr. Stat. Appl. Probab*., vol. 57, CRC Press, Boca Raton, Fla.

Humphreys, E., E. Hessler, K. Dueker, E. Erslev, G. L. Farmer, and T. Atwater (2003), How Laramide-age hydration of North America by the Farallon slab controlled subsequent activity in the western U.S., in *The George A. Thompson Volume; the Lithosphere of Western North America and Its Geophysical Characterization*, *Int. Book Ser.*, vol. 7, edited by S. L. Klemperer and W. G. Ernst, pp. 524–544, Geol. Soc. of Am., Boulder, Colo.

Iglesias, A., V. M. Cruz-Atienza, N. M. Shapiro, S. K. Singh, and J. F. Pacheco (2001), Crustal structure of south-central Mexico estimated from the inversion of surface-wave dispersion curves using genetic and simulated annealing algorithms, *Geofis. Int.*, *40*, 181–190.

Jodicke, H., A. Jording, L. Ferrari, J. Arzate, K. Mezger, and L. Rupke (2006), Fluid release from the subducted Cocos plate and partial melting of the crust deduced from magnetotelluric studies in southern Mexico: Implications for the generation of volcanism and subduction dynamics, *J. Geophys. Res.*, *111*, B08102, doi:10.1029/2005JB003739.

Julià, J., C. J. Ammon, R. B. Herrmann, and A. M. Correig (2000), Joint inversion of receiver function and surface wave dispersion observations, *Geophys. J. Int.*, *143*, 99–112, doi:10.1046/j.1365-246x.2000.00217.x.

Kelleher, J., L. Sykes, and J. Oliver (1973), Possible criteria for predicting earthquake locations and their application to major plate boundaries of the Pacific and the Caribbean, *J. Geophys. Res.*, *78*(14), 2547–2583, doi:10.1029/JB078i014p02547.

Levshin, L., T. B. Yanovskaya, A. V. Lander, B. G. Bukchin, M. P. Barmin, L. I. Ratnikova, and E. N. Its (1989), Recording, identification, and measurement of surface wave parameters, in *Seismic Surface Waves in Laterally Inhomogeneous Earth*, edited by V. I. Keilis-Borok, pp. 131–182, Kluwer Acad., Dordrecht, Netherlands.

Li, A., D. Forsyth, and K. Fischer (2002), Evidence for shallow isostatic compensation of the southern Rocky Mountains from Rayleigh wave tomography, *Geology*, *30*(8), 683–686, doi:10.1130/0091-7613(2002)030<0683:EFSICO>2.0.CO;2.

Menke, W. (1984), *Geophysical Data Analysis: Discrete Inverse Theory*, Academic, Orlando, Fla.

Ordaz, M., and S. K. Singh (1992), Source spectra and spectral attenuation of seismic waves from Mexican earthquakes, and evidence of amplification in the hill zone of Mexico City, *Bull. Seismol. Soc. Am.*, *82*, 24–43.

Pardo, M., and G. Suárez (1995), Shape of the Rivera and Cocos plates in southern Mexico: Seismic and tectonic implications, *J. Geophys. Res.*, *100*(B7), 12,357–12,373, doi:10.1029/95JB00919.

Pedersen, H. A., S. Fishwick, and D. B. Snyder (2009), A comparison of cratonic roots through consistent analysis of seismic surface waves, *Lithos*, *109*, 81–95, doi:10.1016/j.lithos.2008.09.016.

Pérez-Campos, X., Y. Kim, A. Husker, P. M. Davis, R. W. Clayton, A. Iglesias, J. F. Pacheco, S. K. Singh, V. C. Manea, and M. Gurnis (2008), Horizontal subduction and truncation of the Cocos Plate beneath central Mexico, *Geophys. Res. Lett.*, *35*, L18303, doi:10.1029/2008GL035127.

Shapiro, N., M. Campillo, A. Paul, S. K. Singh, D. Jongmans, and F. J. Sánchez-Sesma (1997), Surface-wave propagation across the Mexican

Volcanic Belt and the origin of the long-period seismic-wave amplification in the Valley of Mexico, *Geophys. J. Int.*, *128*, 151–166, doi:10.1111/j.1365-246X.1997.tb04076.x.

Singh, S. K., and M. Pardo (1993), Geometry of the Benioff zone and state of stress in the overriding plate in central Mexico, *Geophys. Res. Lett.*, *20*(14), 1483–1483, doi:10.1029/93GL01310.

Singh, S. K., L. Astiz, and J. Havskov (1981), Seismic gaps and recurrence periods of large earthquakes along the Mexican subduction zone: A reexamination, *Bull. Seismol. Soc. Am.*, *71*, 827–843.

Singh, S. K., J. F. Pacheco, D. García, and A. Iglesias (2006), An estimate of shear-wave *Q* of the mantle wedge in Mexico, *Bull. Seismol. Soc. Am.*, *96*, 176–187, doi:10.1785/0120050001.

Singh, S. K., A. Iglesias, D. García, J. F. Pacheco, and M. Ordaz (2007), *Q* of *Lg* waves in the Central Mexican volcanic belt, *Bull. Seismol. Soc. Am.*, *97*, 1259–1266, doi:10.1785/0120060171.

Suárez, G., J. P. Ligorria, and L. Ponce (1992), Preliminary crustal structure of the coast of Guerrero, Mexico, using the minimum apparent velocity of refracted waves, *Geofis. Int.*, *31*, 247–252.

Valdés-González, C., and R. P. Meyer (1996), Seismic structure between Pacific coast and Mexico City from the Petatlán earthquake (Ms = 7.6) aftershocks, *Geofis. Int.*, *35*(4), 377–401.

Yanovskaya, T. B. (1984), Solution of the inverse problem of seismology for laterally inhomogeneous media, *Geophys. J. R. Astron. Soc.*, *79*, 293–304.

R. W. Clayton, Seismological Laboratory, California Institute of Technology, Pasadena, CA 91125, USA.

D. García, A. Iglesias, X. Pérez-Campos, S. K. Singh, and C. Valdés-González, Departamento de Sismología, Instituto de Geofísica, Universidad Nacional Autónoma de México, Av. Universidad, 3000, Copilco, Del. Coyoacan Mexico City 04510, Mexico. (amg@ollin.igeofcu.unam.mx)

J. F. Pacheco, Observatorio Vulcanológico y Sismológico de Costa Rica, Apartado Postal: 2346-3000 Heredia, Costa Rica.